Arabian Journal of Geosciences (2019) 12: 347
https://doi.org/10.1007/s12517-019-4483-0

REVIEW PAPER

Mapping lateritic bauxite at Az Zabirah, Saudi Arabia, using ground-penetrating radar exploration method

Yasir A. Almutairi[1] · Hesham M. ElAraby[2,3] · Habes A. Ghrefat[2] · Abdulrahman M. Alotaibi[1]

Received: 22 April 2018 / Accepted: 17 April 2019 / Published online: 23 May 2019

Abstract

This paper presents the three-dimensional (3D) data interpretation of a ground-penetrating radar (GPR) survey, in conjunction with the existing boreholes, covering the area of the Az Zabirah bauxite deposits, northern Kingdom of Saudi Arabia. The purpose of this study was to measure and map the volume of the bauxite deposits in the selected survey area, as well as to prove the success of the ground-penetrating radar exploration method in detecting and mapping the bauxite layer. The 3D GPR data interpretation detected the bauxite layer at different depths and of variable thickness. The interpretation of the GPR profiles show three distinct layers, namely sandstone, upper clay, and bauxite of variable thicknesses. Each zone has a different reflection pattern or radar facies, which aided in their differentiation. The calculated total volume of bauxite in the study area from the GPR survey and borehole data was 34,696 m^3 and 34,101 m^3, respectively. The minor difference in the calculated volumes between the two datasets was approximately 1%.

Keywords Ground-penetrating radar · Az Zabirah · Bauxite deposits · Saudi Arabia · Mapping · Borehole

Introduction

Bauxite deposits originated from weathering or soil formation with an abundant of aluminum. Bauxite is used in the abrasives, chemical, and refractory industries. The igneous, metamorphic, or sedimentary rocks are the parent rocks of bauxite (Kusuma 2012). Bauxite deposits are composed of a mixture of gibbsite $Al(OH)_3$, boehmite γ-AlO(OH), diaspore α-AlO(OH), goethite and hematite, kaolinite clay, and small amounts of titanium dioxide. According to Fahad et al. (2009), bauxite also contains magnetite, siderite, ilmenite, rutile, brookite, halloysite, and quartz.

Ninety percent of the world's bauxite reserves are concentrated in tropical and semi-tropical regions. Australia is the leading bauxite producer followed by China, Brazil, and Guinea (Table 1). Australia also possesses several of the highest-grade deposits with nearly 50% available alumina content. The Saudi Arabian Mining Company (Ma'aden) has been progressively expanding its bauxite operations between Al-Qassim and Hail in 2001 since the discovery of more than 90 million tons (mt) of bauxite at Al-Zabirah (Alcoa Inc. 2012).

The US Geological Survey (USGS 2014) in 1963, after conducting geological mapping and surveying of many locations in Saudi Arabia, reported the occurrence of "laterite clay and bauxite" north of Qiba City. The complete geological evaluation of these deposits was accomplished by Riofinex, geological and geophysical consultants, via an exploration drilling program from 1979 to 1984. The Az Zabirah bauxite deposit was discovered during exploration of the Aruma Formation. To provide data for geostatistical assessment, Riofinex conducted an exploration program of the Az Zabirah deposit that involved a reconnaissance study with regional mapping, outcrop and channel sampling, regionally spaced drilling, and additional close-spaced drilling. Riofinex drilled a total of 331 holes in the south, central, and northern zones of the Az Zabirah bauxite deposit. The bauxite deposits

Editorial handling: Abdullah M. Al-Amri

✉ Habes A. Ghrefat
habes@ksu.edu.sa

[1] King Abdulaziz City for Science and Technology, Riyadh, Saudi Arabia

[2] College of Science, Geology and Geophysics Department, King Saud University, Riyadh, Saudi Arabia

[3] Faculty of Science, Geophysics Department, Cairo University, Cairo, Egypt

Table 1 World production of bauxite from 2016 to 2017 (USGS 2018)

Country	Mine production (mt/year)		Reserves (mt/year) (2017)
	2016	2017	
Australia	82,000	83,000	6,000,000
China	65,000	68,000	1,000,000
Brazil	34,400	36,000	2,600,000
Guinea	31,500	45,000	7,400,000
Saudi Arabia	3840	3900	210,000

had formed during the Early Cretaceous because of the weathering of Late Triassic to Early Jurassic terrigenous sediments deposited in marine or littoral environments.

As part of the feasibility study and in conjunction with the Saudi Deputy Ministry of Mineral Resources (DMMR), geoscientists from the Bureau de Recherches Géologiques et Minières (BRGM) conducted a three-stage drilling program between 1987 and 1993, referred to as the 1993-BRGM study. During 1990, BRGM completed a closely spaced cross-drilling program in the central zone to support the preliminary geostatistical evaluation undertaken by Riofinex.

In 1991, 128 holes were drilled on a nominal 500 m × 500 m grid in the central and south zones and by the end of 1992, the number of test holes approached 233 in these zones with the same nominal spacing. Regional mapping was conducted around Az Zabirah by DMMR-BRGM teams and resulted in the preparation of two reference maps at a 1:250,000 scale (Lebret et al. 1999; Robelin et al. 1994). Furthermore, these maps indicated that the bauxite deposits occur discontinuously along a strike of about 5 km width and a length of about 105 km.

In 1999, following a competitive tender, Ma'aden was authorized to complete the feasibility of the Az Zabirah bauxite deposit. A preliminary technical and economic evaluation was completed (Hatch 2008) and 389 test holes were drilled to demarcate the mineral resources of the south and central zones. An additional 604 test holes targeted the south zone in 2003 to measure the bauxite resources according to the guidelines of the 1999 Joint Ore Reserves Committee (JORC) code that had been previously inferred by Hatch 2008. A trial mining operation for a feasibility study commenced in 2003 with 97 reverse circulation (RC) drill holes for grade control. Other investigations were completed by the Saudi Arabian Bechtel Company in 2004 followed by a supplementary geology and mining study by SMG Consultants (Pty) Ltd. in early 2005. The technical audit for geology and mine planning was independently performed by SRK in 2005.

Hatch (2008) completed a pre-feasibility study for the establishment of an integrated bauxite–alumina–aluminum project. This was conducted via extensive infill drilling within the previously delineated area of bauxite ore for the determination of sufficient reserves to support the funding requirement for the development of the project. According to Ma'aden, the bauxite resource in the south zone will support a world class mining, refining, and aluminum metal project for at least the next 50 years.

Ground-penetrating radar (GPR) has been used since the 1990s for mapping a variety of mining, geological, geotechnical, and environmental studies. GPR was used to measure the ice thickness (Steenson 1951; Evans 1963; Bryan 1974; Behrendt et al. 1979; Bently et al. 1979); map bedrock structures in underground mines (Cook 1973, 1975, 1977; Dellwig and Bare 1978); and find the location of hidden pipes and utilities (Morey 1974, 1976; Caldecott et al. 1988; Osumi and KUeno 1988). GPR is a non-destructive tool that can be utilized in archeological investigations (Ulriksen 1982; Imai et al. 1987; Davis and Annan 1989; Hänninen 1992; Daniels 2004). According to Austin and Austin (1974) and Ulriksen (1982), GPR has been used in measuring the depth of shallow water. GPR has also been tested in mineral resources of limestone quarrying, placer deposits, kimberlites, laterite and bauxites, iron ore deposits, and sand deposits (Frankce 2012; Erten et al. 2013).

The aim of this study was to map a three-dimensional (3D) image of a certain part of the bauxite layer in the Az Zabirah area using GPR to prove the suitability of this geophysical method for bauxite exploration in this area, which could increase the speed of production and the value of bauxite ore in this part of the world.

Location and geological setting of the study area

The study area is located in the stable shelf in which the marine sedimentary rocks dominate the Arabian Platform (Fig. 1). The Az Zabirah bauxite deposits are near Az Zabirah (27° 55′ N and 43° 41′ E) in the northern part of Saudi Arabia, 180 km to the north of Buraydah and 100 km northwest of Qiba town. An NW-SE strike of extends for about 90 km and dips for about 1° to the northeast characterizes the area of study.

The bauxite deposits made up the sedimentary layers of the eastern Najd. These layers are aligned northwest to southeast between the sand dunes and sand sheets of the An Nafud (to the south) and the Ad Dahna (to the north). The lower boundary of the Az Zabirah bauxite is along an angular unconformity where the Late Cretaceous rocks (Wasia and Aruma formations) overly the clastic sediments of Late Triassic, Early-Middle Jurassic, and Early Cretaceous age. According to Bowden (1981) and Black et al. (1982), the stratigraphic units in the study area are equivalent to the Minjur, Marrat, Dhruma, Tuwaiq, and Biyadh formations. The bauxite profile extends as outcrops for approximately 125 km along the strike of the

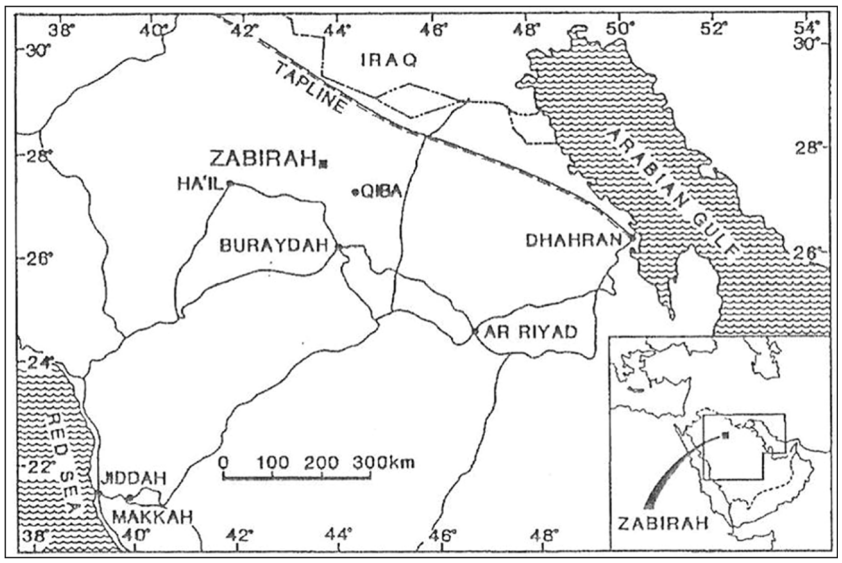

Fig. 1 Location map of the study area (Black et al. 1982)

overlying rock units with some erosional discontinuities (Fig. 2). The discontinuity in the geologic exposures of the bauxite deposits at Az Zabirah distinguishes three different zones: the north, central, and south zones (Black et al. 1982). The most prominent topographic feature of the Az Zabirah area is a northwest-to-southeast-aligned limestone escarpment, 50 to 80 m in height (Aruma Formation). The bauxite outcrops are found between distinct low plateaus and shallow escarpments. These bauxite escarpments are usually no more than 10 m in height. However, they may exceed 20 m at some locations. Plains of residual origin, alluvial plains (mostly along wadies), dunes, and sand sheets formed from eolian-deposited sands can be found between the plateaus. Quaternary active sheet sands and the dunes of the Irq Al Mazhur (which rise up to 100 m above ground level) form the boundary of the bauxite deposits to the southwest. As previously mentioned, the bauxite deposits are sub-divided into north, central, and south zones to facilitate exploration of the resource (Fig. 2).

The bauxite deposits comprise a Cretaceous paleolaterite that has been uplifted and exposed to erosion during the quaternary. They occur within a Mesozoic sedimentary sequence. The sequence is represented by the Triassic to Jurassic Jihl, Tuwaiq Mountain, Minjur, Marrat, and Dhurma formations, respectively, with the Biyadh Sandstone (Lower Cretaceous) and the Wasia and Aruma formations (Upper Cretaceous) (Ross et al. 1984) (Fig. 3). The Mesozoic sedimentary sequence was deposited on a stable platform without any major tectonic disturbances subsequent to the Cambrian (Powers et al. 1966). The unevenly eroded bauxite assemblage (lower clay, bauxite, and upper clay zones) is covered by the Upper Cretaceous Wasia Formation and Aruma Limestone on the northeastern flank of the deposit.

The sequence of the south zone of the bauxite represents a laterite profile and is subdivided into three zones from the bottom to the top as follows: The lower clay (LCZ), the pisolitic bauxite (BXZ), and the upper clay (UCZ) zones are the three subdivisions of the south zone of bauxite. This zone represents a laterite profile. The maximum thickness of the bauxite profile is approximately 10 m with an average of 6 m (Fig. 4). The commercial bauxite is limited to The BXZ and UCZ zones which are of economic values, whereas the LCZ is categorized as sub-economic. Figure 5 shows a typical laterite bauxite profile in the study area (Black et al. 1982).

The thickness of the LCZ ranges from 2 to 5 m. The LCZ mainly consists of erratic clay with sheets of white, purple, blue, reddish-brown, gray, or green-gray color. The upper level of this zone may include considerable pisolitic formation that closely resembles the bauxite to the touch. The bedrock is composed of ferruginous mudstone that is relatively non-permeable and the formation of the bauxite deposits is distinct along the joints and stratified sheets. This has resulted in the development of successive stages of clay brecciated-bauxite in which remains of the angular mudstone float in a matrix made of pisolitic bauxite or tubular bauxite where vertical tubes of the pisolitic bauxite penetrate the original non-transformed mudstone and the mudstone that contains isolated white patches.

The length of BXZ is approximately 15 km. It trends NW-SE from the Sabkhas basin escarpment, some 9 km northwest of Al Bi'ithah, continuing through the village for approximately 6 km to the southeast. According to Black et al. (1982), the BXZ is associated with tubercles of sandy limestone but may have also been welded by calcareous material.

A thin layer of very rigid ferruginous material that occurs directly above the bauxite could cover other vast areas. The bauxite zone thickness ranges between 0 and 3 m and is overlain by the UCZ. The most prominent bauxite outcrops are encountered along the northeastern slope of the Sabkhas basin, where the thickness of the exposures is 2 m. The BXZ is

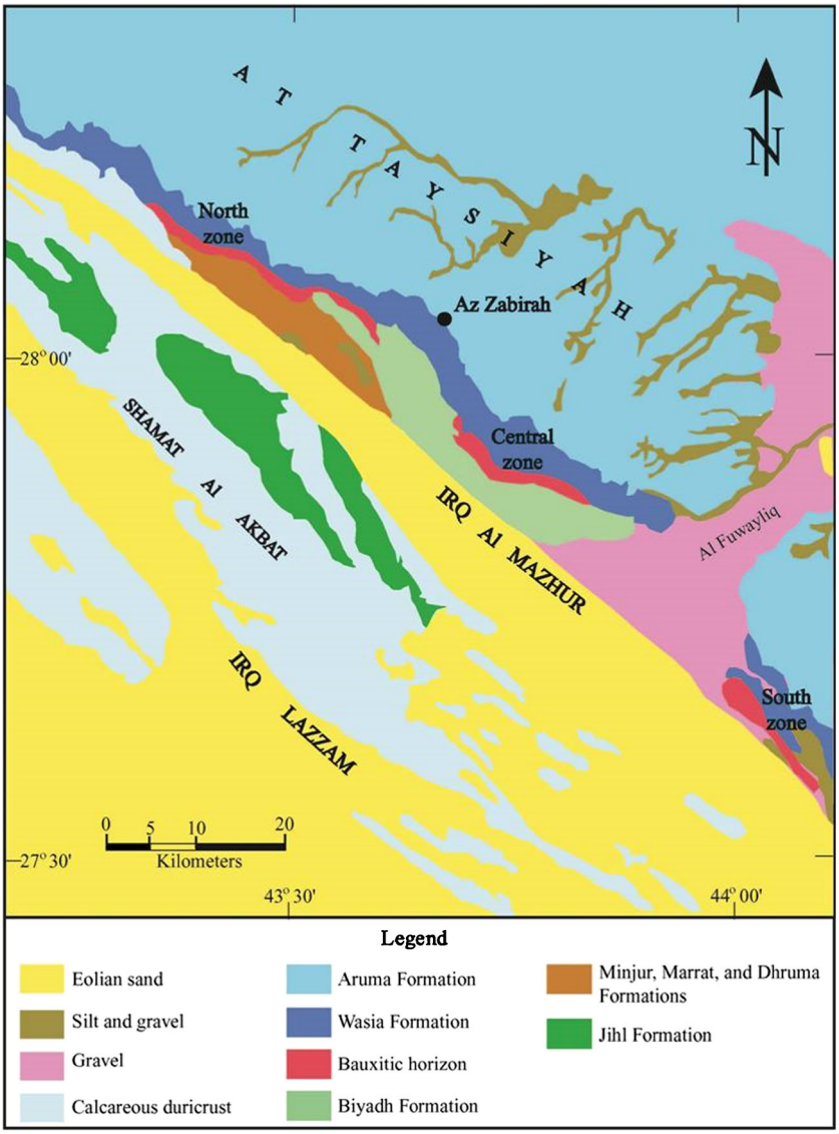

Fig. 2 Geological map of the three zones of Az Zabirah bauxite deposits (Black et al. 1982)

mainly composed of iron oxides and ranges from a sharp contact to a wavy surface (Fig. 6).

Layers of pisolitic hematite of a red or reddish-brown color with a thickness of approximately 15 to 20 cm were discovered within the bauxite zone. At some locations, the thickness of the hematite layers may reach 40 cm, while in others, it can be completely eroded. There is an approximately 1-m-thick layer of detrital reddish bauxite underlying the hematitic bauxite. This is entirely composed of oolitic to pisolitic grains cemented by a bauxitic and/or kaolinitic matrix. Clasts of pisolitic bauxite to hematitic bauxite of reddish to brown color characterize the bauxite layers in the other parts of the study area.

A hard micro-oolitic to pisolitic bauxite layers overlies the kaolinitic pisolitic bauxite. The thickness of these layers range from about 50 cm to 1 m. The color of bauxite is deep brown to reddish brown. The bauxitic conglomerate are made up of reddish to reddish brown pisoliths and ooliths. It is formed of highly ferruginous, very hard medium to coarse pisoliths that are deep brown to reddish brown and attain a thickness ranging from 50 cm to 1 m. These are composed of reddish to reddish brown pisoliths and ooliths. The bauxitic conglomerate grades into hard reddish brown microolitic to oolitic bauxite and reddish-brown macro-pisolitic to pseudo breccia.

The UCZ is characterized by a pisolitic touch, and consists of clay and bauxitic clay. The thickness of this zone varies between 0.5 and 2 m and may be partially or completely eroded in some locations. In this case, the bauxite zone directly overlies the top of the sandstone of the lower Wasia formation. The original surface of the lateritic zone covering the upper clay zone is characterized by a rigid layer rich in iron and varying in thickness between 0.2 and 0.3 m. The UCZ represents the re-silicified uppermost part of the bauxite zone in which the original pisolitic texture of the bauxite has been locally preserved (GHD 2005).

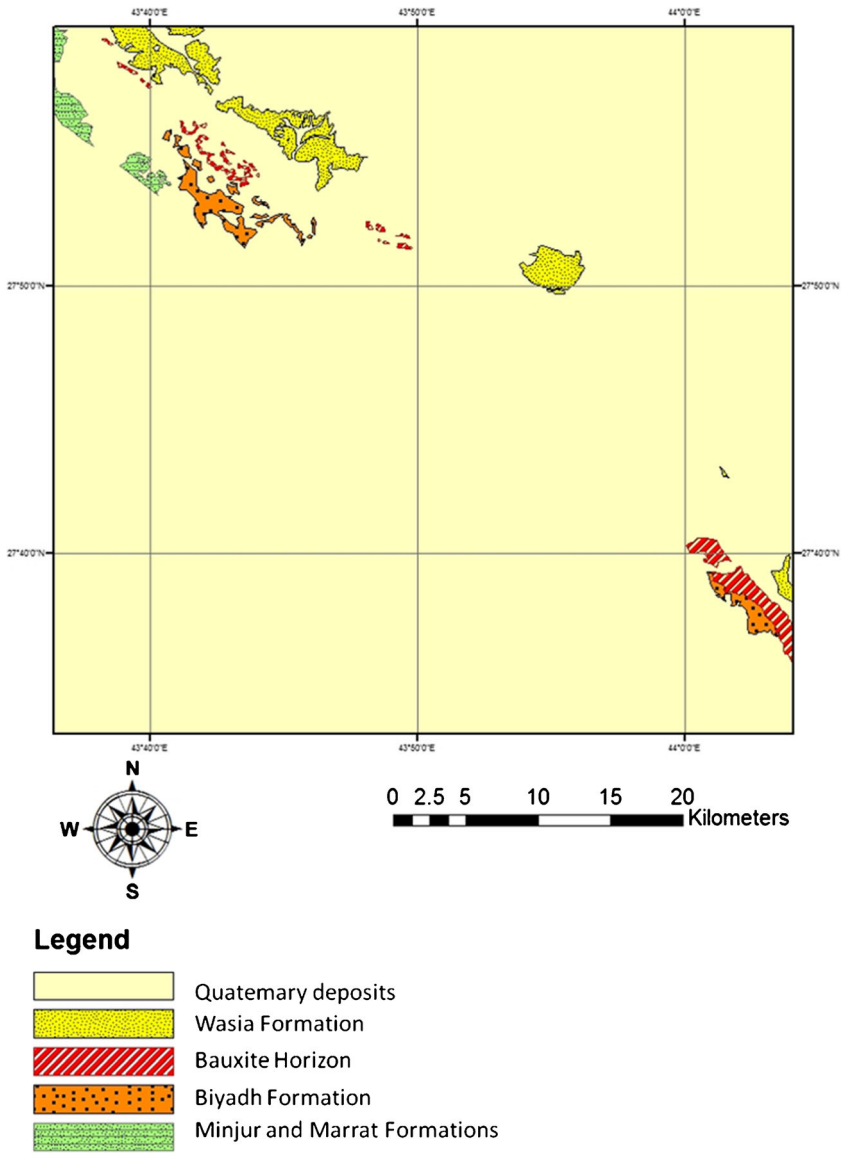

Fig. 3 Geological map of the Az Zabirah south zone bauxite

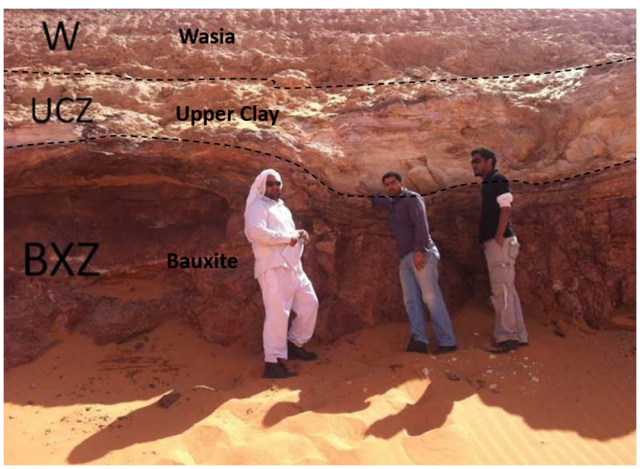

Fig. 4 The sequence profile of bauxite deposits in the study area

The Wasia Formation is of Late Cretaceous age and is characterized by a periodic internal structure accompanied by deposits representing alternating phases of continental and shallow marine environments. The surface layer is composed of sandstone with a thickness of 4 m followed by a clay layer with a variable thickness ranging from 0 to 1 m and a bauxite layer at a depth range from 5 to 10 m.

GPR basic concept, acquisition, and processing

A transmitter and a receiver connected to an antenna and a control unit are the three major component of the GPR system (Fig. 7). A short high frequency of electromagnetic pulses (typically radio waves ranging from 1 to 1500 MHz

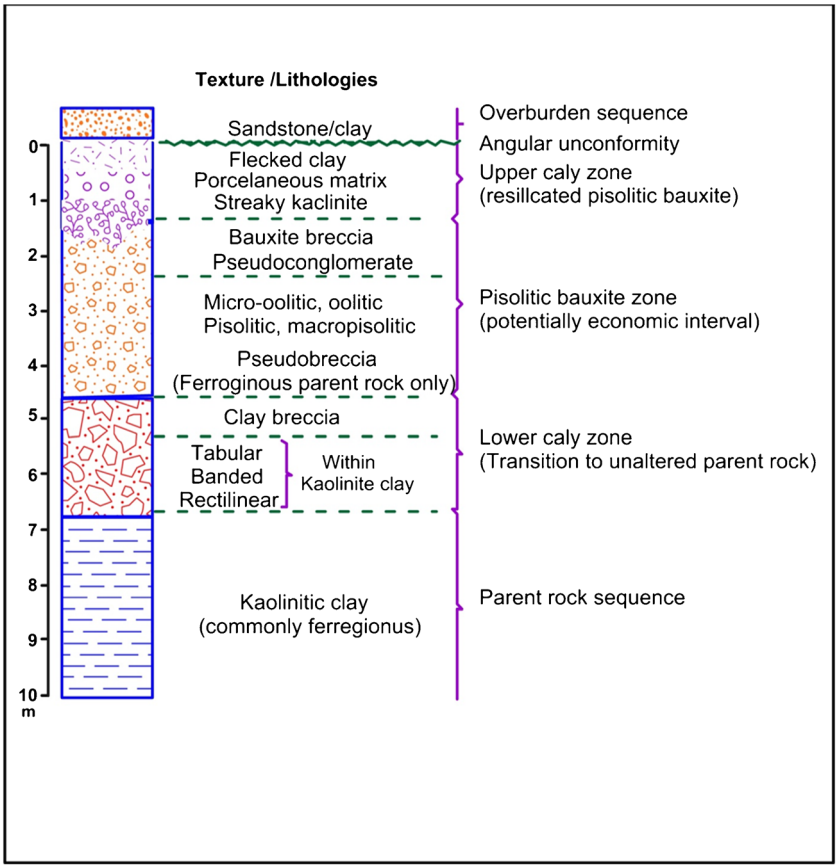

Fig. 5 A typical bauxite profile developed in the study area (Black et al. 1982)

frequency) radiates into the ground from the transmitter. The waves are refracted and reflected because they encounter changes in dielectric parameters and electric conductivity (Basson 2000). According to Gawthorpe et al. (1993), the reflected waves back to the surface is detected by a receiver antenna that measures the two-way travel time.

GPR is effective when the medium has low electrical conductivity, such as ice (0.01 mS/m), sand (0.01 mS/m), limestone (0.5–2 mS/m), and fresh water (0.5 mS/m). In contrast, it is less effective when the medium has high electrical conductivity, such as wet clay (2–1000 mS/m), silt (1–100 mS/m), and saline water (3000 mS/m). Changes in subsurface

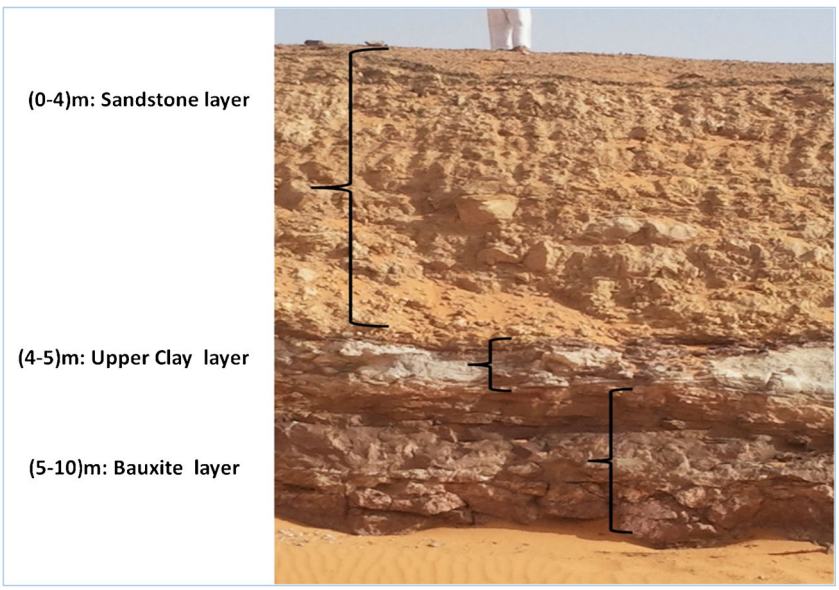

Fig. 6 Stratigraphic cross section shows the lithological units and corresponding depth and thickness at study area

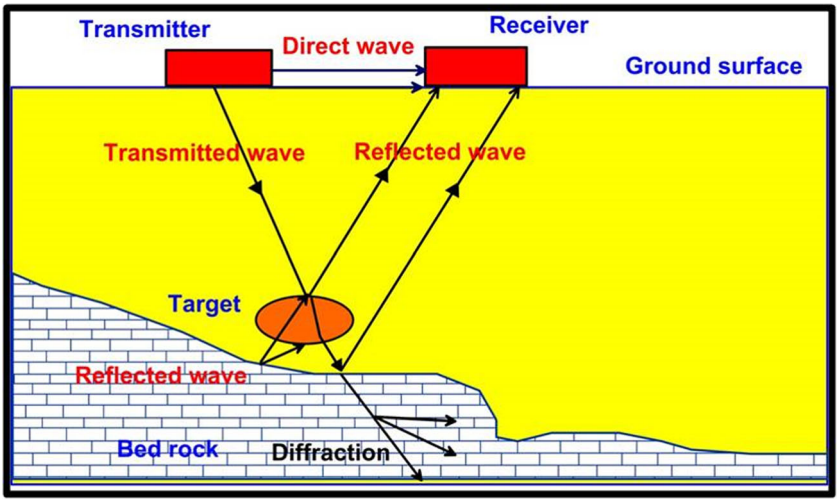

Fig. 7 GPR system components (Basson 2000)

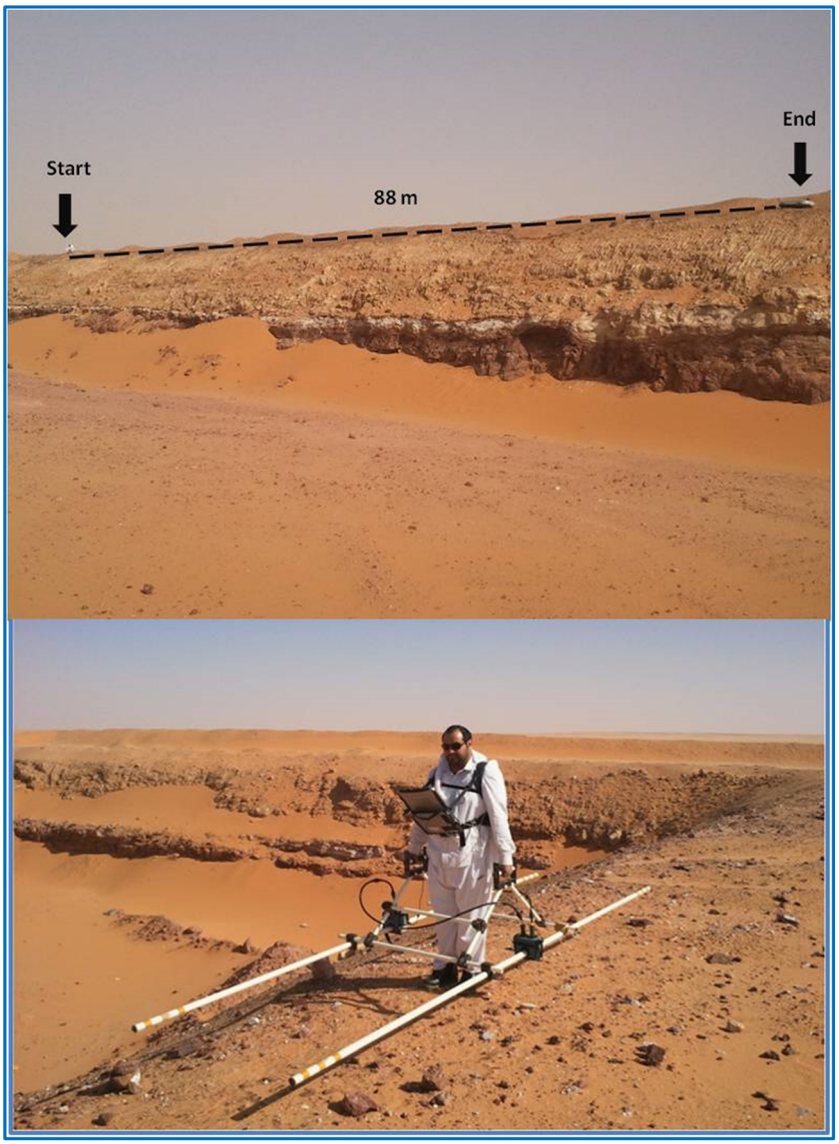

Fig. 8 **a** Data acquisition system; **b** Test profile

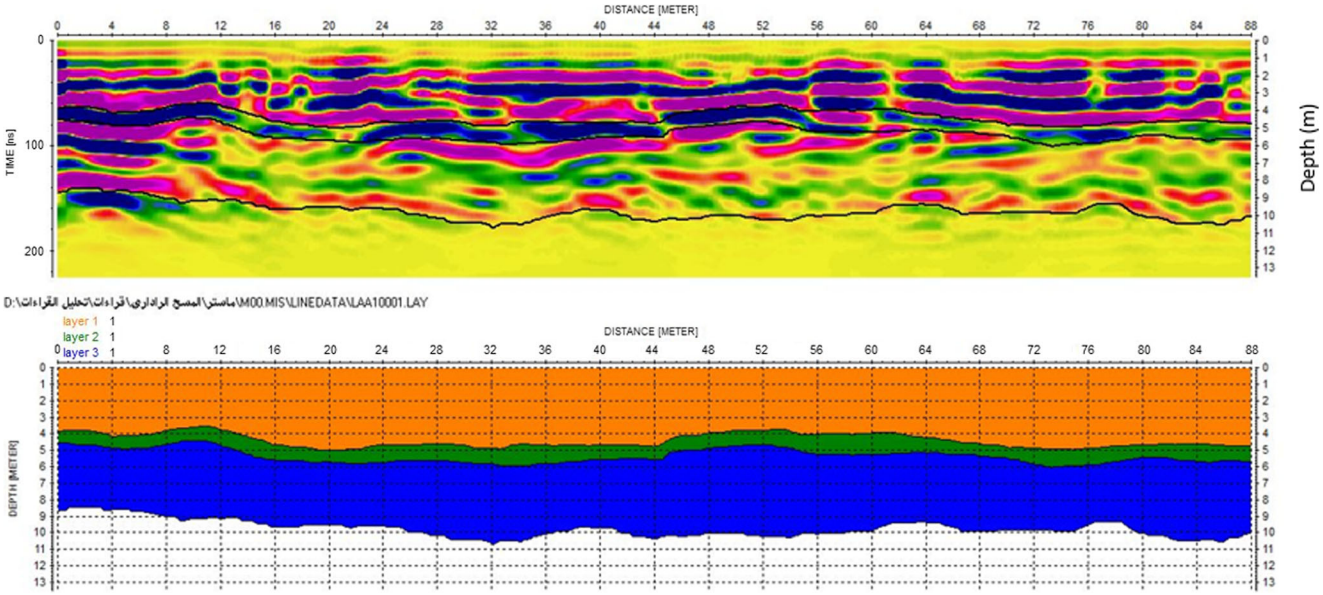

Fig. 9 Interpreted GPR test profile measured over the trial pit (upper) and its corresponding layer (lower)

electrical properties are caused by changes in the physical characteristics of the subsurface material. According to Davis and Annan (1989), the conductive soils attenuate the radar signals more than the resistive soils. The penetration depth of GPR depends on different parameters including the antenna frequency, dielectric constant, and the electrical conductivity of the soils. The low-frequency antennas have low spatial resolution and can penetrate greater depths than those of high-frequency antennas (Reynolds 1997). Antenna frequency is a major factor in depth penetration. The higher the frequency of the antenna, the shallower into the ground it will penetrate (Davis and Annan 1989). A higher frequency antenna will also see smaller targets. Antenna choice is one of the most important factors in survey design (Hänninen 1992). We

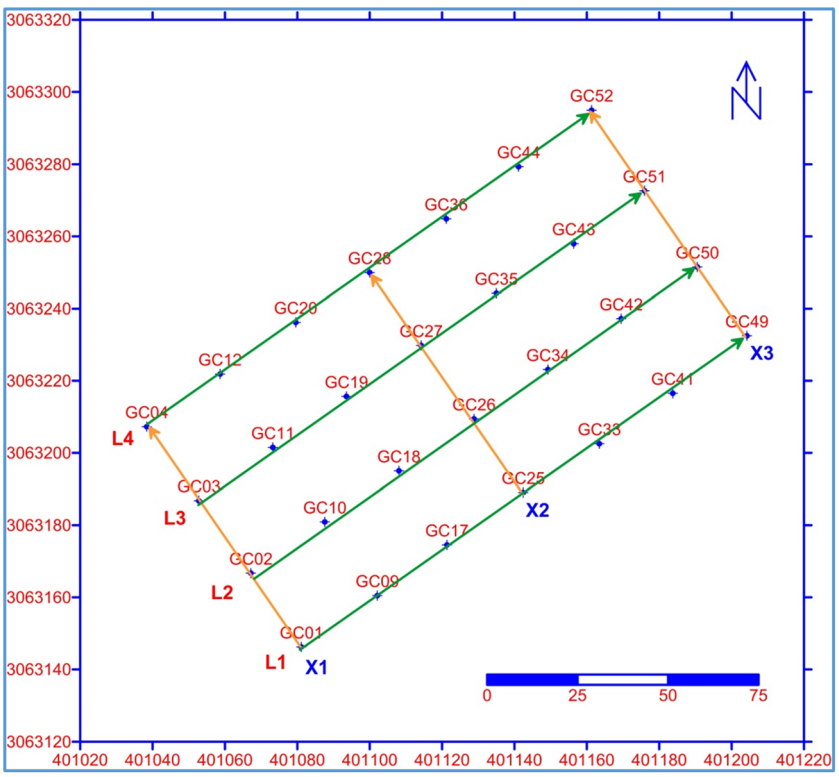

Fig. 10 Location map of the study area

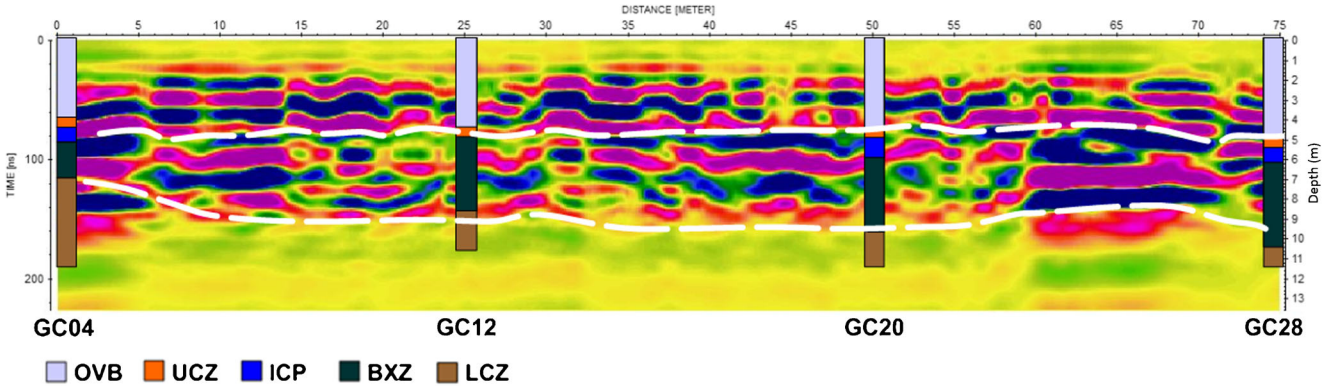

Fig. 11 Stratigraphic interpretation of GPR section L1 from 0 to 75 m OVB, UCZ, ICP, BXZ, LCZ

have decided to use a 25-MHz frequency antenna for better resolution of the subsurface and also to get more penetration to grantee the imaging of the bauxite layer.

The vertical resolution depends primarily of the wavelength (λ) of the propagating electromagnetic wave, which is determined by the GPR frequency (f) and velocity (v) of the ground material as $\lambda = v/f$. Theoretically, the distance between two reflectors should at least be (¼–½)of the wavelength to be resolved (Sheriff 1987), though in practice, the distance should be (½–1) wavelength (Møller and Vosgerau 2006). Using a ½ wavelength, the vertical resolution in dry sand with a velocity of 0.15 m/ns is about 3 m, 1.5 m, 0.75 m, and 0.19 m for a 25 MHz, 50 MHz, 100 MHz, and 400 MHz center frequency, respectively. In saturated sand with a lower velocity of about 0.06 m/ns, the vertical resolution is 1.2 m, 0.6 m, 0.3 m, and 0.075 m for a 25 MHz, 50 MHz, 100 MHz, and 400 MHz center frequency, respectively.

A GPR survey was conducted using the IDS GPR system with a central frequency of 25 MHz antenna. The components of the GPR system consisted of a DAD control unit, notebook computer, lane cable, battery cable, and battery pack (Fig. 8a). The collected data may be converted into depth/x-y location as needed with relative ease. Such an instrument may be carried at rates of up to 10 miles/h, making GPR an immediately practical large-area survey tool.

For the purposes of the preliminary investigation and velocity determination, the 25-MHz central frequency antenna was used to provide a reasonable image of the near surface region and the deep penetration depth that could provide a good image of the bauxite layer. The measurements were conducted over the exposure (Fig. 8b) and velocity determination is done using the true depth measured on the exposure section in the field.

However, the data showed several problems. In many profiles, there is horizontal banding running across the image as a result of the less-than-optimal coupling of the antenna to the ground and unwanted oscillatory ringing of the antenna. GPR in areas composed of a fragmented sandstone and compact sandstones shows a good signal-to-noise ratio. A good correlation is observed between the raw radar sections and the stratification of the geological formations (Fig. 9). The results of the current study demonstrated that the value of signal-to-noise ratio is decreased in areas of intense and thick clay layers. The electromagnetic wave velocity was calculated using the depth to the bauxite surface as measured from the trial pit. The primary interpretation of the test shows major bounding surfaces of the sandstone layer and bauxite layer (blue) also observed in the trial pit photo (Fig. 9).

We created a grid with seven profiles to cover the survey site (Fig. 10). Four GPR lines trending to the NE (L1–L4) with a line spacing of 25 m and a profile length of 150 m were established. Furthermore, three lines directed towards the NW

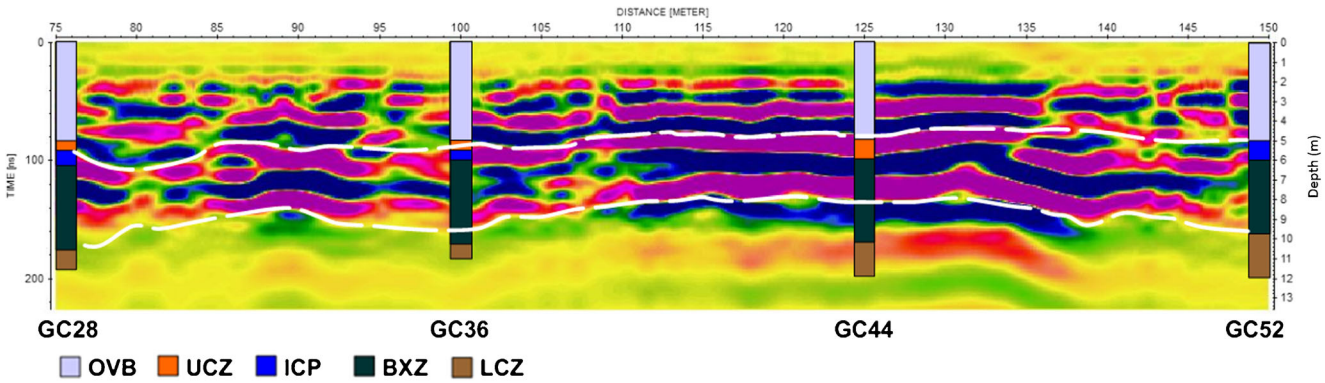

Fig. 12 Stratigraphic interpretation of GPR section L1 from 75 to 150 m OVB, UCZ, ICP, BXZ, LCZ

Table 2 A comparative study between the computed depth from GPR and borehole data along line L1

Line L1							
Distance	0 m	25 m	50 m	75 m	100 m	125 m	150 m
Borehole name	GC-04	GC-12	GC-20	GC-28	GC-36	GC-44	GC-52
Thickness of clay layer	0.5	0.5	0.5	0.5	0.5	1.0	0.0
Bauxite borehole depth	4.5	5.0	5.0	5.5	5.5	6.0	5.0
Bauxite calculated depth	4.7	4.8	4.6	5.1	5.25	4.5	5.1
% of error	4.4	4.0	8.0	7.2	4.5	25.0	2.0

(X1–X3) with a line spacing of 75 m and profile length of 75 m were established. Data processing was carried out using the Reflex 6.0 software (Sandmeier 2010).

In the GPR data processing, common steps were followed as described below:

(A) Signal processing

Before starting the processing steps, we have assumed the velocity value to be 0.13 m/ns; this was based on the trial pit results and it is equivalent to a vertical resolution of 2.6 m for the 25-MHz frequency used. The general objective of signal processing as applied to surface-penetrating radar is either to present an image that can be readily interpreted by the operator or to classify the target return with respect to a known test procedure or template. A series of tests were carried out for frequency filtering on a sample of radar sections, which was considered to better represent the entire set of data. The tests carried out for this research followed some standard procedures; nevertheless, where it was necessary, some alternative actions or reiterations of the standard procedures were chosen. We have applied all the processing steps on the raw data of the test profile.

(B) Time cut

This filter acts on each trace independently. The processing step time cut offers the possibility to limit each trace to a pre definable maximum time. In our data we have applied a maximum time of 250 ns and we have removed the remaining time window.

(C) Declipping plateau

It is common in ground-penetrating radar (GPR) imagery to have missing or corrupted traces. This can be either due to obstacles, noise, technical problems, or economic considerations. Antenna-ground coupling is another reason for clipped amplitudes in GPR data.

(D) Subtract-Mean (dewow)

This running mean is subtracted from the central point. This is a temporal filtering for the removal of very low frequency components (de-wowing) from the data. The filter calculates a running mean value for each trace and subtracts it from the central point. This filter acts on each trace independently. This option activated a running mean value is calculated for each value of each trace.

(E) Moving start time

This filter is applied to remove the arte facts in the data. The time zero must be set at the first-energy arrival, and for these kinds of measurements, the first arrival characterizes the interface air-ground. The time zero is also a function of the system timing, cable lengths, and antenna positioning.

(F) Adjusting the gain

The manual gain has been applied in the *Y*-direction, This filter acts on each trace independently. The option allows to

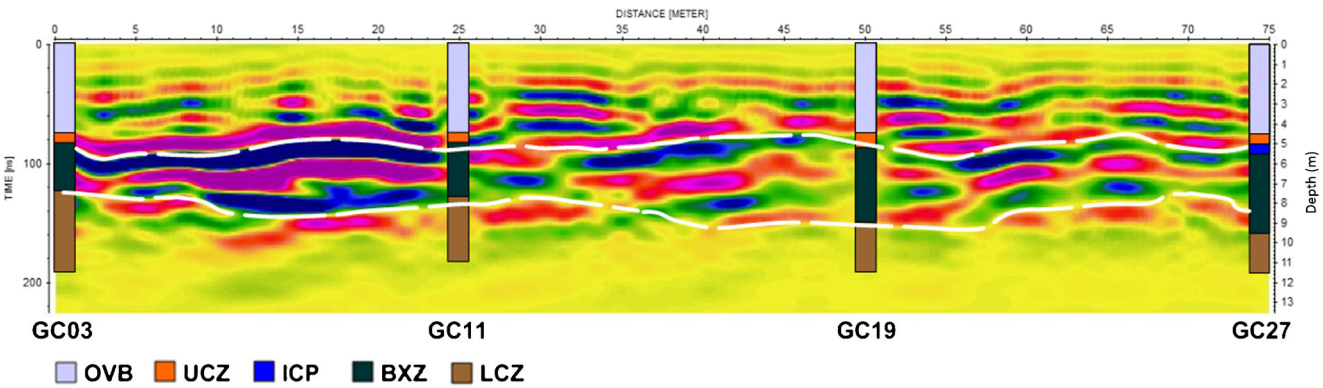

Fig. 13 Stratigraphic interpretation of GPR section L2 from 0 to 75 m OVB, UCZ, ICP, BXZ, LCZ

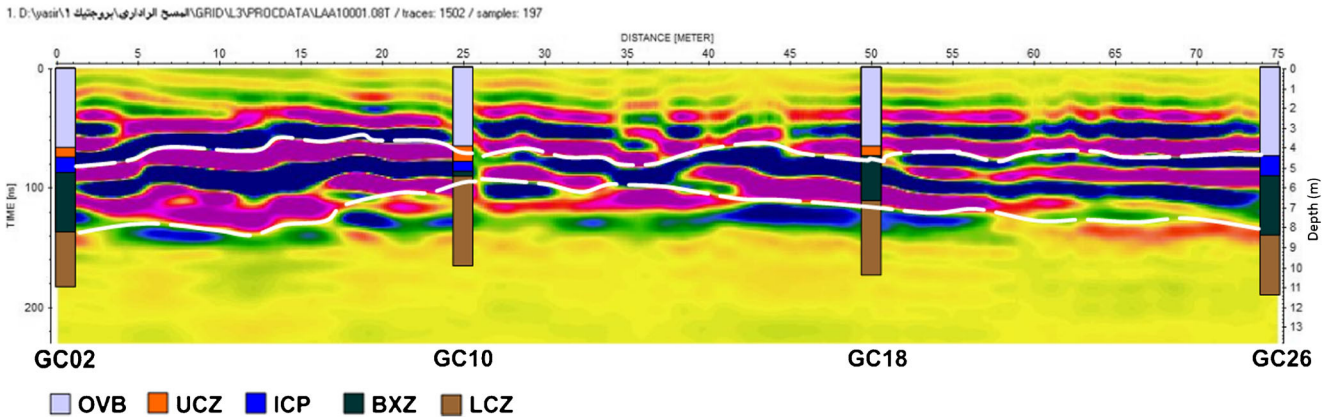

Fig. 14 Stratigraphic interpretation of GPR section L3 from 0 to 75 m ☐ OVB, ■ UCZ, ■ ICP, ■ BXZ, ■ LCZ

interactively define a digitized gain curve in time axis and to apply this gain curve on the data.

(G) Background removal

The average of all the scans, which have been accumulated, can be removed using the background removal filter in order to eliminate the antenna ringing and horizontal banding across the image. This part of the processing enables an efficient radar image enhancement and it can be applied in different phases of the processing itself for 25-MHz antenna measurements.

(H) Band pass butterworth filter

The butterworth filter is a type of signal processing filter designed to have as flat as frequency response as possible in the pass band. The filter acts on each trace independently in which the lower cutoff frequency was kept at 12 MHz and upper cutoff was 72 MHz. The frequency spectrum below the low cut and above the high cut was set to zero.

(I) Average *x*-*y* filter

The average is performed both over a number of traces (*x*) and over a number of samples (*y*). The filter area is centered around the current data point to obtain a smooth average of arrival times from the bottom. The start time is set to the begin time of each trace and end time is set to the max.

Results and discussion

The data interpretation for all the GPR lines (L1–L4 and X1–X3) demonstrated the depth of the bauxite layer. All lines illustrated three separate zones or horizons as well as their thicknesses. Each zone showed a different reflection pattern or radar facies, which helped in differentiation. The first horizon composed of sandstone is the superficial layer; the second is a diffraction zone, which corresponds to the upper clay layer; and the third showed discontinuous reflectors, which correspond to the main bauxite horizon (BXZ).

The interpretation of GPR section L1 shows that the bauxite deposits were imaged at depths exceeding 10 m with an excellent correlation with the boreholes. The distinguished layer of bauxite has a thickness of approximately 2.3–5.25 m, which is in the range of the method vertical resolution for the specific velocity determined in the field and the used antenna frequency. The variation in thickness is due to the slight variations of electromagnetic

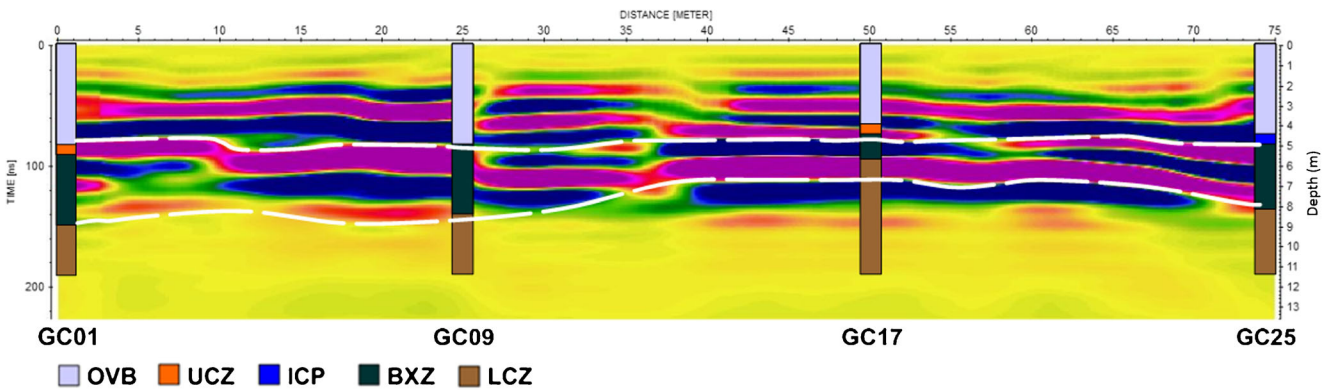

Fig. 15 Stratigraphic interpretation of GPR section L4 from 0 to 75 m ☐ OVB, ■ UCZ, ■ ICP, ■ BXZ, ■ LCZ

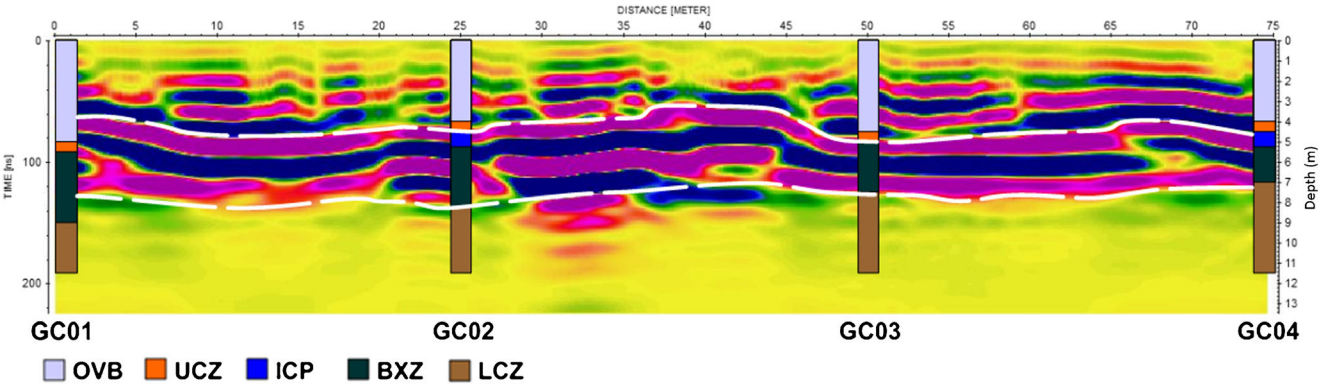

Fig. 16 Stratigraphic interpretation of GPR section X1 OVB, UCZ, ICP, BXZ, LCZ

properties of the medium. Figure 11 shows a part of the line from the starting point to a horizontal distance of 75 m reflecting the general lithological homogeneity of the bauxite. Meanwhile, Fig. 12 shows the second half of the GPR section along line L1 starting from a horizontal distance of 75 to 150 m. Table 2 shows a comparative study between the results obtained by the GPR and those obtained from borehole data; the percentage of errors in our calculations are also tabulated.

For line L2, the upper surface of the bauxite was mapped at a depth range between 5 and 6.30 m, whereas its lower surface was imaged at a depth of 7.5–9.5 m, which conforms with that of the boreholes, where the error in the depth is approximately 50 cm. The distinguishing layer of bauxite has thicknesses of approximately 2.85–4 m (Fig. 13).

The GPR section of line L3 shows that the bauxite deposits have an upper surface at a depth of nearly 4 m and they extend to a depth of 8 m, which correlates well with the boreholes (Fig. 14). The GPR section of line L4 shows that the bauxite deposits have an upper surface at a depth of nearly 4.5 m and they extend to a depth of 8.25–10.5 m, which correlates well with the boreholes (Fig. 15).

Interpretation of transverse line X1 shows the upper and lower surfaces of the bauxite layer where its thickness ranges between 2.2 and 3.7 m (Fig. 16). The interpretation of the X2 GPR profile indicates the upper and lower surfaces of the bauxite layer, where its thickness ranges between 3.7 m and 5 m. The GPR section of line L4 shows that the bauxite deposits have an upper surface at a depth of 5.1–6.25 m and they extend to a depth of 8.25–9.75 m, which correlates well with the boreholes.

The upper and lower boundaries of the identified bauxite layer were drawn as 3D surfaces (Fig. 17). The minimum depth to the upper surface is 3.2 m while that to the lower surface is 5.6 m. The maximum depth to the upper surface is 6.9 m and that to the lower surface is 10.7 m. The total volume of the bauxite layer in the survey area is approximately 34,696 m^3. The GPR-mapped bauxite layer shows a complicated shape in terms of depth and thickness.

Conclusions

The GPR data provides an accurate estimation of the expected bauxite volume that represents valuable information of production estimation and economical evaluation. The GPR identified bauxite upper and lower surfaces were presented as 3D surfaces that enable the calculation of the total volume of the bauxite. GPR data in conjunction with boreholes data have emphasized the efficiency to map three layers: sandstone, clay, and the bauxite (BXZ), and

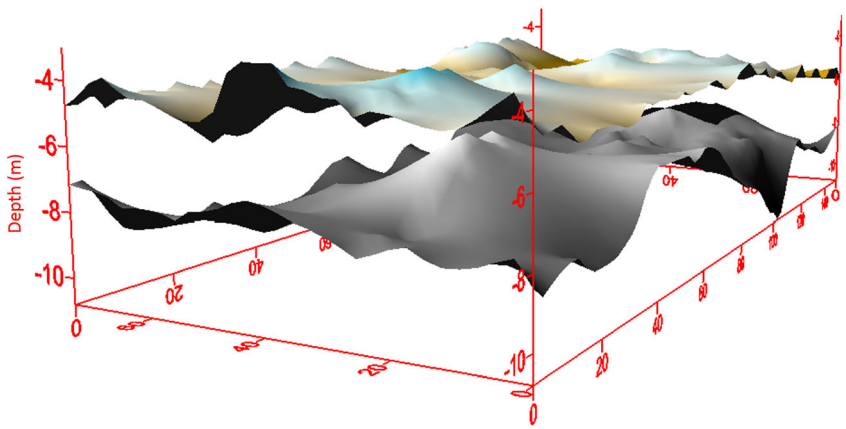

Fig. 17 3D presentation of the GPR identified bauxite upper and lower surfaces

have calculated their thickness. The use of GPR in bauxite resource evaluations greatly reduces the cost of drilling with saturation coverage.

Acknowledgements The authors would like to thank King Abdulaziz City for Science and Technology and the Ma'aden Company for their scientific support and assistance during the field work. Appreciation is also extended to colleagues Khaled Almutairi, Abdulaziz Almutairi, Ramzi Almutairi, and Abdulsalam Alasmari (King Abdul-Aziz City for Science and Technology) for their help and support.

References

Alcoa Inc. (2012) Ma'aden Alcoa aluminum joint venture pours first concrete for Middle East's first alumina refinery at Ras al Khair: Riyadh, Saudi Arabia, Alcoa Inc news release, February 3.

Austin GL, Austin LB (1974) The use of radar in urban hydrology. J Hydrol 22:131–142

Basson U (2000) Imaging of active fault zone in the Dead Sea Rift: Evrona Fault Zone as a case study: thesis submitted for the degree of PhD, Tel-Aviv University, Raymond & Beverly Sackler, Faculty of Exact Sciences, Department of Geophysics and Planetary Sciences, 196 p

Behrendt JC, Drewry D, Jankowski E, England W (1979) Aeromagnetic and radar ice sounding indicate substantially greater area for dufek intrusion in Antarctica. Antarct J US 60:245

Bentley CR, Clough LW, Jezek KC, Shabtaie S (1979) Ice thickness patterns and the dynamics of the Ross Ice Shelf, Antarctica. Journal oj' Glaciology 24:287–294

Black RY, Bognar B, Watson AD, Barnes DP (1982) Evaluation of the Az Zabira bauxite deposit (1980–1982). Riofinex Ltd., Tech. Rep

Bowden RA (1981) Geology of the Az Zabira bauxite occurrence. Riofinex Ltd., open file report

BRGM Geoscientists (1993) Az Zabirah bauxite deposit prefeasibility study—technical report BRGM-TR-13-3, Part 1: Ministry of Petroleum and Mineral Resources—directorate general of mineral resources

Bryan ML (1974) Ice thickness variability on Silver Lake, Genesee County, Michigan: a radar approach, advanced concepts in the study of snow and ice resources: United States contribution to the international hydrological decade, 213–223

Caldecott R, Poirier M, Scofea D, Svoboda DE, Terzuoli AJ (1988) Underground mapping of utility lines using impulse radar. Institute of Electrical Engineers, Proceedings F. communications, radar and signal processing 135 part F. pp 343–361

Cook JC (1973) Radar exploration through rock in advance of mining. Transactions of AIME: Society of Mining Engineers 254:140–146

Cook JC (1975) Radar transparencies of mine and tunnel rocks. Geophysics 40:865–885

Cook JC (1977) Borehole-radar exploration in a coal seam. Geophysics 42:1254–1257

Daniels DJ (2004) Ground penetrating radar 2nd edition – London: the Institute of Electrical Engineers United Kingdom

Davis JL, Annan AP (1989) Ground penetrating radar for high resolution mapping of soil and rock stratigraphy. Geophys Prosp 37:531–551. https://doi.org/10.1111/j.1365-2478.1989.tb02221.x

Dellwig LF, Bare JE (1978) A radar investigation of North Louisiana salt domes. Photog Eng Remote Sens 44:1411–1419

Erten O, Kizil MS, Topal E, McAndrew L (2013) Spatial prediction of lateral variability of a laterite-type bauxite horizon using ancillary ground-penetrating radar data. Nat Resour Res 22(3):207–227. https://doi.org/10.1007/s11053-013-9210-z.

Evans S (1963) Radio techniques for the measurement of ice thickness. Polar Record 11:406–410

Fahad M, Iqbal Y, Ubic R (2009) Bauxite deposits in Pakistan: an introduction: J Pak Mater Soc 2009 3(1):41–44.

Frankce J (2012) A review of selected ground penetrating radar applications to mineral resource evaluations. J Appl Geophys 81:29–37

Gawthorpe RL, Collier RE, Alexander J, Bridge JS, Leeder MR (1993) Ground-penetrating radar-application to sandbody geometry and heterogeneity studies. Geochem Soc Spec Publ 73:421–432

GHD (2005) Ma'aden Aluminuim project: terms of reference for environmental impact assessment

Hänninen P (1992) Application of ground penetrating radar and radio wave moisture probe techniques to peatland investigations. Geological Survey of Finland, Rovaniemi, Finland, 71 pp

Hatch (2008) Ma'aden/Alcan Az Zabirah aluminium project: mine and refinery FEL 2 study—mine operating plan—document no: 327197-M20-T-24-0004 MA ADEN NO M100–1-RE-003 Rev 0 Report submitted to Ma'aden

Imai T, Sakayama T, Kanemori T (1987) Use of ground penetrating radar and resistivity surveys for archeological investigations. Geophysics 52:137–150

Kusuma KN (2012) Spectral pathways for effective delineation of high-grade bauxites: a case study from the Savitri River basin, Maharashtra, India, using EO-1 Hyperion data. Int J Remote Sens 33(22):7273–7290

Lebret PM, Halawani A, Memesh P, Razin C, Bourdillon D, Janjou Y, Nindre Y-ML, Roger J, Shorbaji H, Kurdi H (1999) Geologic map of the Turubah quadrangle, sheet 28F, Kingdom of Saudi Arabia, scale 1:250,000. Ministry of Petroleum and Mineral Resources, Geoscience Map GM-139, with explanatory notes

Møller I, Vosgerau H (2006) Testing ground penetrating radar for resolving facies architecture changes—a radar stratigraphic and sedimentological analysis along a 30 km profile on the Karup Outwash Plain, Denmark. Near Surface Geophysics 4(1):57–68

Morey RM (1974) Continuous sub-surface profiling by impulse radar: conference on subsurface exploration for underground excavation and heavy construction. American Society of Civil Engineers, pp 213–232

Morey RM (1976) Detection of subsurface cavities by ground penetrating radar. Highway Geological Symposium 27:28–30

Osumi N, Ueno K (1988) Detection of buried plant. IEE Proceedings F Communications. Radar and Signal Processing 135(4):330

Powers RW, Ramirez LF, Redmond LD, Elberg EL (1966) Sedimentary geology of Saudi Arabia U.S. Geol. Surv., Prof. Pap. 560-D

Reynolds JM (1997) An introduction to applied and environmental geophysics: Chichester

Robelin C, Al-Muallem MS, Brosse JM, Fourniguet J, Garcin M, Gouyet JF, Halawani M, Janjou D, Nindre Y-ML (1994) Geologic map of the Qibah quadrangle, sheet 27G, Kingdom of Saudi Arabia, scale 1:250,000. Ministry of Petroleum and Mineral Resources, Geoscience Map GM-136, with explanatory notes

Ross Y, Black RY, Lozej GP, Maddah SS (1984) Geology and mineralogy of the Az Zabirah bauxite, northern Saudi Arabia: proceedings of the 1984 bauxite symposium, Los Angeles

Sandmeier KJ (2010) Reflex 6.0 Manual. Sandmeier Software. Zipser Strabe 1, D-76227 (Karlsruhe, Germany)

Sheriff RE (1987) Exploration seismology: Volume 2, Data-processing and interpretation. Cambridge University Press, Cambridge

Steenson BO (1951) Radar methods for the exploration of glaciers Pasadena, California: California Institute of Technology, Pasadena

Ulriksen CP (1982) Application of impulse radar to civil engineering: Published PhD Thesis, Lund University of Technology, Lund, Geophysical Survey Systems, Inc. Hudson, New Hampshire, 179 p

USGS (2014) US geological survey: http://minerals.usgs.gov/minerals/pubs/commodity/bauxite/index.html#myb